Available online at www.sciencedirect.com

ScienceDirect

Advances in Space Research 77 (2026) 7168–7182

ADVANCES IN SPACE RESEARCH (a COSPAR publication)

www.elsevier.com/locate/asr

Spacecraft electrostatic tractor using a power-constrained pulsed high-energy high-current electron beam

Amy Haft *, Hanspeter Schaub [1]

Ann & H.J. Smead Department of Aerospace Engineering Sciences, 3775 Discovery Dr, Boulder 80303, United States

Received 3 November 2025; received in revised form 15 December 2025; accepted 15 January 2026
Available online 21 January 2026

Abstract

The electrostatic tractor is a concept for debris removal and detumbling in geosynchronous Earth orbit (GEO), where a servicer spacecraft directs an electron beam (e-beam) at a debris target. The servicer becomes positively charged through electron emission, while the target charges negatively upon impact, generating an attractive electrostatic force. This force enables the servicer to gradually re-orbit the debris into a graveyard orbit. Previous studies using continuous e-beams show that this force is on the order of milli-Newtons or less, requiring several months to achieve the necessary change in velocity. This paper investigates how a pulsed e-beam, at the same average power, can significantly enhance the electrostatic force if sufficient current is delivered. High-energy electrons are emitted for a short pulse such that, over the duty cycle, the same mean power is consumed as a lower energy beam that is continuously on. High electrostatic potentials can result in field emission, but these are shown to be manageable. Additionally, a space-weather-dependent optimal duty cycle that maximizes the electrostatic force is presented. By increasing the achievable force, the required re-orbit time can be reduced by one to two orders of magnitude, with even greater reductions possible under stronger e-beam parameters. Pulsed e-beam performance is evaluated across a range of representative GEO space weather conditions.

Keywords: Spacecraft charging; Debris remediation; Electrostatic tractor

1. Introduction

Spacecraft in high Earth orbit are known to charge naturally to kilovolt levels due to currents from the local plasma, such as ambient electron and ion currents or the photoelectron current when in sunlight (Lai, 2011, Chapter 1). Because of the sparse and energetic nature of the plasma environment at high altitudes, such as in geosynchronous Earth orbit (GEO), spacecraft may charge to severe negative potentials on the order of thousands to tens of thousands of volts while in eclipse (DeForest, 1972). The ATS-6 satellite, for example, experienced record charging up to −19 kV in GEO (Olsen, 1987). Although spacecraft charging is often regarded as a risk due to deep dielectric discharge and differential charging concerns, previous studies demonstrate the promise of active spacecraft charging at high altitudes as a means to re-orbit defunct satellites (Schaub and Moorer, 2012; Hughes and Schaub, 2015a; Schaub and Sternovsky, 2014; Aslanov, 2020; Aslanov and Yudintsev, 2018) or detumble spacecraft prior to servicing them (Trevor Bennett et al., 2015; Bennett and Schaub, 2015; Bennett and Schaub, 2018; Stevenson, 2016; Aslanov, 2019; Aslanov and Schaub, 2018). Active spacecraft charging refers to the deliberate

E-mail addresses: Amy.Haft@colorado.edu (A. Haft), Hanspeter.Schaub@colorado.edu (H. Schaub).
[1] Distinguished Professor and Department Chair.

https://doi.org/10.1016/j.asr.2026.01.050

use of a non-natural currents, commonly from an electron gun on a servicer spacecraft, to charge a nearby target. This generates controlled potentials on both spacecraft and results in attractive and repulsive forces between them (Ting et al., 2016; Tahir and Narang-Siddarth, 2018; Yamamoto and Yamakawa, 2008). GEO is a particularly suitable environment for active charging because the Debye length, a measure of how far a charged object's electrostatic effect persists, is on the order of hundreds of meters, compared to centimeters in low Earth orbit (LEO) (Champion and Schaub, 2023; Leahy, 2021; Guillemant et al., 2012; Anderson, 2012).

The proposed method for contactless space debris re-orbiting is the Electrostatic Tractor (ET) (Schaub and Moorer, 2012). Here, a servicer spacecraft equipped with an ancillary propulsion system uses an electron beam (e-beam) to make the potential of a target object negative while its own potential becomes increasingly positive. Eventually, the servicer's positive potential grows large enough such that some emitted electrons are attracted back to the servicer and the net currents on both the servicer and target due to the e-beam and space environment reach a net zero current steady state equilibrium condition. The electric potential of a spacecraft when the net current is zero is the equilibrium potential. The resulting attractive force allows the servicer to re-orbit the target. The servicer's propulsion system must then provide the inertial force to achieve the necessary change in velocity ΔV to put both spacecraft onto a transfer orbit and then into the final graveyard orbit.

To maintain the electrostatic force between spacecraft, the thrust force provided by the propulsion system cannot be significantly larger than the electrostatic force (Hogan and Schaub, 2013). Thus, maximizing the electrostatic force improves mission efficiency. Previous research primarily used a continuous e-beam to calculate the electrostatic force, and found results on the order of a few milli-Newtons or less (Hammerl and Schaub, 2024b; Haft and Schaub, 2024). In some studies, the e-beam parameters were varied for a range of plasma conditions to find the optimal combination of beam energy and current to maximize the e-tractor force (Hughes and Schaub, 2015b). In contrast, Refs. Hughes and Schaub (2017b) and Hughes and Schaub (2017a) investigated if a pulsed e-beam can result in an increase in force. The theory predicted that, for a given mean power consumption, it is possible to achieve much higher averaged e-tractor forces by using a high-voltage, high-current e-beam for a fraction of the time in cycles on–off pulses. This is compared to the original e-tractor concept where a lower current, lower voltage e-beam is on for the duration and uses the same mean power. Because the force increases roughly quadratically as a function of spacecraft potential, the pulsed beam theoretically can result in a higher electrostatic force than a continuous beam. A challenge identified in the earlier work is the time it takes for a pulse to reach an equilibrium charging condition.

The studies conducted in Refs. Hughes and Schaub (2017b) and Hughes and Schaub (2017a) present an interesting baseline for the pulsed beam e-tractor concept. While results show that the pulsed beam can increase the force, the effect is not optimized as a function of the duty cycle, which is the ratio of time that the e-beam is turned on to the total period of the pulse. Instead, Ref. (Hughes and Schaub, 2017b) focuses on optimizing the electrostatic force by varying the tuning parameter, which determines the ratio of e-beam current to e-beam voltage. The effect of local time during quiet conditions is also observed, and storm conditions are looked at for specific parameters. The e-beam is simulated only at duty cycles of 10 %, 25 %, 50 %, and 100 % (continuous case). As a result, the full effect of the power-limited pulsed e-beam is not explored. The study also does not account for multiple populations of plasma particles in the GEO environment, instead only using a single-Maxwellian distribution of particles. The GEO environment plays a significant role in the effectiveness of the ET, so it is necessary to build upon this work with an increasingly realistic model.

The purpose of this research is to employ the coupled spacecraft effects to determine if there exists an optimal duty cycle such that the electrostatic force is maximized. Of interest is investigating if new emerging electron guns with high currents and rapid response times could lead to a better power constrained e-tractor performance. For example, the company Think Orbital is developing a novel space-based welding system that can sustain high currents and has a fast response time.[2] While Think Orbital uses very short separation distances for the welding, our application would spread out the beam over a larger distance such that the target receives the high current without melting issues.

A key concern of the power-constrained pulsed e-tractor concept is that it takes a finite time for space objects to charge to their equilibrium state. This is a function of the e-beam properties and the local space environment. If the charging time is too long compared to the pulsed beam on-time, then the resulting electrostatic force would be small. This paper first studies how the duty cycle can be used to optimize the electrostatic force in eclipse. Because the electron gun pulsing cycles are result in higher currents and energies being considered, significant charging occurs and field emission must be considered. This paper investigates if field emission is a significant concern for the potentials being considered. The research study is compared to the continuous electron beam. The effect the photoelectron current has on optimal pulsed beam charging is then determined. Next, the changing GEO plasma environment is taken into account, and the pulsed beam is simulated at various geomagnetic storm strengths and times compared to local midnight. The charging simulations are conducted using a bi-Maxwellian flux distribution of hot and colder

[2] https://thinkorbital.com

plasma to emulate a more complex and realistic space environment than what was considered in prior work. Finally, a brief study on how the electron beam power can be modified to overcome limiting environmental effects is conducted.

2. Electrostatic re-orbiting background

2.1. Electrostatic tractor force modeling

To quantify the electrostatic force in such a way that the effects on the GEO debris re-orbiting mission can be fully understood, it is useful to approximate the re-orbit time t_{burn} to go from the GEO altitude to the GEO disposal orbit. Fig. 1 illustrates the electrostatic force acting on the servicer and the target object. The servicer is assumed to have an inertial thruster generating the force F_T (Hogan and Schaub, 2013; Schaub and Moorer, 2012) to maintain a constant separation distance between vehicles. While the time-varying e-tractor has been considered to detumble a large debris object prior to docking, without loss of generality this paper focuses on the tugging application where a sustained net electrostatic force is the goal.

The electrostatic force F_E acts between the servicer and the target. This force is calculated by first using the relationship between electric potentials ϕ_S (servicer) and ϕ_T (target) and charges Q_S and Q_T between two spacecraft modeled here as charged spheres: (Smythe, 1968; Stevenson and Schaub, 2013)

$$\begin{bmatrix}\phi_S\\ \phi_T\end{bmatrix} = k_c\begin{bmatrix}1/R_S & 1/d\\ 1/d & 1/R_T\end{bmatrix}\begin{bmatrix}Q_S\\ Q_T\end{bmatrix} \tag{1}$$

The variables R_S and R_T are the radii of each sphere, d is the separation distance between them, and k_c is the Coloumb constant equal to 8.988×10^9 $(\text{N}\cdot\text{m}^2)/\text{C}^2$. Then, F_E can be found using the Coloumb equation

$$F_E = k_c\frac{Q_S Q_T}{d^2} \tag{2}$$

The radii R_S and R_T are approximated using Eq. (3), which provides a first-order relationship between the mass of the spacecraft and their radii (Schaub and Jasper, 2013). In this study the servicer mass is $m_S = 500$ kg, which allows it to fall into the category of medium sized GEO satellite. The resulting equivalent sphere radius is $R_S = 1.5$ m. The equivalent sphere maps the actual capacitance of a complex spacecraft shape to a representative sphere with the same capacitance (Schaub and Jasper, 2013). Additionally, the target space object mass is $m_T = 4276$ kg, which is the average mass of a newly launched GEO satellite as of 2014 (Ostrove, 2015). The resulting equivalent sphere radius is $R_T = 4$ m. The radii of the spherical spacecraft are calculated from the following trend equation developed in Schaub and Jasper (2013)

$$R_{S,T} = 1.152\text{m} + 0.00066350\,\frac{\text{m}}{\text{kg}}m_{S,T} \tag{3}$$

The capacitance of each satellite is estimated from its shape and size and then represented with a sphere of equivalent capacitance.

Previous continuous e-beam research shows electrostatic forces between spacecraft on the order of mN or less (Hammerl and Schaub, 2024b; Haft and Schaub, 2024). This poses an interesting challenge for the ET concept. To achieve a net ΔV system to re-orbit the servicer-debris system, F_T must be greater than F_E. The F_T required to keep the tug ahead of the debris by a fixed separation distance is(Hogan and Schaub, 2013; Schaub and Moorer, 2012)

$$F_T = \frac{m_S + m_T}{m_T}F_E > F_E \tag{4}$$

This condition results in both servicer and debris to accelerating by the same amount. Here m_S and m_T are the masses of the servicer and target respectively (Schaub and Moorer, 2012). The small F_T required to maintain F_E means that t_{burn} will be sizable. However, a larger F_E would allow for a larger F_T, and thus a larger F_{net}.

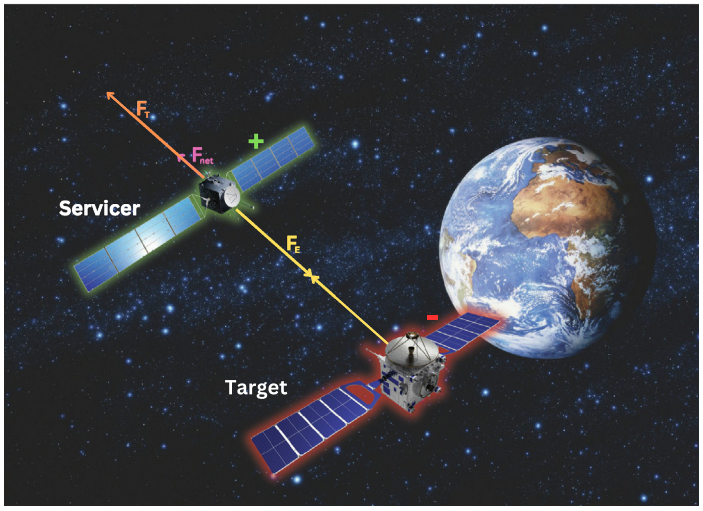

Fig. 1. Electrostatic tractor concept with forces visualized.

To further quantify results in this research, F_T can also be written in terms of t_{burn}:

$$F_T = \frac{m_{\text{prop}} I_{\text{sp}} g_0}{t_{\text{burn}}}, \tag{5}$$

where g_0 is the standard gravity (9.80665 m/s^2), I_{sp} is the specific impulse of the propulsion system, and m_{prop} is the mass of the burned propellant equal to

$$m_{\text{prop}} = m_S \left(1 - \exp \frac{-\Delta V}{I_{\text{sp}} g_0}\right). \tag{6}$$

2.2. E-Beam Power

Assuming that the ET is equipped with an e-beam with some fixed power specification P, it is of interest to determine if it is optimal to use this power continuously at some given e-beam current I and e-beam voltage V, or if pulsing the e-beam such that I and V are increased during a short time period will maximize the electrostatic force for the same P. The fixed electric power P is given by

$$P = IV \tag{7}$$

where I is the current and V is the potential. If the e-beam is pulsed, then the power equation becomes $P = \mathscr{D} \cdot I_p V_p$ where $\mathscr{D}$ is the duty cycle. To maintain the power specification, I and V must be

$$I_{\text{p}} = \frac{\gamma I}{\sqrt{\mathscr{D}}} \tag{8}$$

and

$$V_{\text{p}} = \frac{V}{\gamma \sqrt{\mathscr{D}}} \tag{9}$$

which can be substantially larger than the I and V for the continuous beam depending on $\mathscr{D}$. A tuning parameter γ is included in these equations, where $\gamma > 1$ indicates that current increase more than voltage and $\gamma < 1$ suggests the opposite. In this study, a $\gamma = 1$ value is used because this was found to be optimal in Hughes and Schaub (2017b), which found that a maximum force was produced when $\gamma \approx 1$ at both high and low duty cycles. Using this approximation allows the current study to focus on maximizing the electrostatic force with respect to the duty cycle alone. These augmented e-beam properties can cause the magnitude of the potential of both the target and servicer spacecraft to be amplified. This means that the resulting electrostatic force may be increased by using a pulsed beam that uses the same mean power as the continuous e-beam solution. The pulsing mechanism used in this study is "on–off" pulsing, meaning that the e-beam will be switched entirely off and back on during one pulsing cycle.

2.3. Charging model

The charging model employed here is based on the one developed in Hammerl and Schaub (2024a). This charging model assumes fully-conducting spherical spacecraft. It also assumes that the only coupled charging effect is due to the e-beam. Accounting for the secondary and back-scattered electrons from the negatively charged target being attracted to the positively charges servicer is left for future work. Moreover, attraction of the plasma particles uses an orbit-limited approximation, which means the flux is calculated as that incident on a sphere of the same potential and depends only on the surface potential (Davis et al., 2016). The net current on the servicer and the target are each

$$\begin{aligned} I_{\text{net}} = {} & I_e + I_i + I_{\text{beam}} + I_{\text{BS}_e} + I_{\text{BS}_{\text{beam}}} + I_{\text{SE}_e} + I_{\text{SE}_p} \\ & + I_{\text{SE}_{\text{beam}}} + I_{\text{PE}}. \end{aligned} \tag{10}$$

where I_e is the ambient electron current, I_i is the ambient ion current (assumed to be Hydrogen nuclei), I_{beam} is the e-beam current, I_{BS_e} is the back-scattered electron current due to ambient electrons, $I_{\text{BS}_{\text{beam}}}$ is the back-scattered electron current due to the e-beam, I_{SE_e} is the secondary electron current due to ambient electron impact, I_{SE_p} is the secondary electron current due to ambient ion impact, $I_{\text{SE}_{\text{beam}}}$ is the secondary electron current due to e-beam impact, and I_{PE} is the photoelectron current. The equations for these currents are dependent on the servicer potential ϕ_S and the target potential ϕ_T and can be found in Hammerl and Schaub (2024a). The time varying potential of both the servicer and target spacecraft is found by numerically solving the differential equation

$$\begin{bmatrix} \frac{\mathrm{d}\phi_T}{\mathrm{d}t} \\ \frac{\mathrm{d}\phi_S}{\mathrm{d}t} \end{bmatrix} = \frac{1}{4\pi\varepsilon_0} \begin{bmatrix} \frac{1}{R_T} & \frac{1}{d} \\ \frac{1}{d} & \frac{1}{R_S} \end{bmatrix} \begin{bmatrix} I_{\text{net}_T}(\phi_T) \\ I_{\text{net}_S}(\phi_S) \end{bmatrix} \tag{11}$$

where d is the distance between the spacecraft.

2.4. Bi-Maxwellian plasma environment

Prior research on optimizing the electrostatic tractor in different GEO environments uses a single-Maxwellian flux distribution function (FDF)(Hammerl and Schaub, 2024a; Hughes and Schaub, 2015b) or accounts for only one population of particles (Hughes and Schaub, 2017b). However, the plasma environment at GEO can be composed of two or more particle populations. This study uses the Denton bulk GEO plasma properties (Denton et al., 2005) where a cold and dense population of plasmasphere particles is used, as well as a hotter, more tenuous population of particles injected from the magnetotail. Both populations vary depending on solar storm activity and the local time LT. The colder plasma component will impact the charging and discharging response times in this pulsed charging scenario. One way of measuring solar storm activity is by using the planetary K index, or Kp index. Higher values of Kp index correspond to greater geomagnetic activity, with values of $Kp \geqslant 5$ indicating a solar storm. When the magnetosphere is compressed as a result of solar activity, magnetotail particles are accelerated to high energies and injected into GEO. Magnetotail particles are also acceler-

ated during substorms, and the electron flux is enhanced between local midnight and dawn as a result of the eastward drift of the injected high energy electrons. The result is a plasma environment that is more accurately represented by a bi-Maxwellian flux distribution function (FDF) represented by $f(E)$, which accounts for both the cold plasmasphere particles and the hot injected particles as a function of energy E. Each population is modeled using a Maxwellian FDF, and their sum is the bi-Maxwellian FDF

$$f(E) = f_1(E) + f_2(E) \tag{12a}$$

$$f_{1,2}(E) = n_{1,2}\left(\frac{q_0}{2\pi m T_{1,2}}\right)^{1/2} \frac{E}{T_{1,2}} \exp\left(-\frac{E}{T_{1,2}}\right) \tag{12b}$$

where q_0 is the unsigned elementary charge, n is the particle density, T is the particle temperature, m is the mass of the particle, and E is energy. The subscript 1 indicates the cold population, and 2 indicates the hot population.

Altitude is often denoted in terms of L shell, where the value of L represents the number of Earth radii above the center of the Earth. For example, $L = 1$ is at the Earth's surface. During quiet times, the plasmapause can extend out as far as $L = 7$, fully encompassing GEO at $L = 6.6$, but geomagnetic activity causes the plasmasphere to compress significantly (Pierrard et al., 2021). Within the plasmasphere, electron density decreases exponentially with altitude until reaching the plasmapause, where the electron density is around 100 cm^{-3} (Laakso et al., 1997). The plasmasphere electrons have low energies, generally in the range of 1 to 10 eV (Williams, 1985). Outside of the plasmapause, the density of these low-energy electrons decreases by orders of magnitude (Laakso et al., 1997). In this paper, the density of the cold electrons at GEO will be modeled as 100 cm^{-3} for $Kp = 0$ (no solar activity) and 1 cm^{-3} for $Kp = 2, 4$, and 6. This assumption aligns with the equation for the plasmapause location as a function of Kp index in Pierrard et al. (2021). This paper neglects the effects of day/night variations on the electron density, thus, the cold electron density does not vary with local time. The energy of the cold electrons used in this paper is 1 eV for all Kp indices.

All the positive ions are assumed to be H nuclei. The densities and energies for the cold ions, hot ions, and hot electrons are taken from Denton et al. (2005). The energy of the cold ions is assumed to be 50 eV, since the study measures cold ions as all ions with energies between 1 and 100 eV. The density of the cold ions varies with Kp index and LT. The hot particle population's densities and energies also vary with both Kp and LT.

3. Force increases due to duty cycle

The goal of this work is to maximize the electrostatic tractor force F_E while holding the mean e-gun power consumption constant. The continuous (nominal) e-beam current is $I = 520\mu A$ to keep consistent with Hughes and Schaub (2015b). The continuous beam energy used here is $E = 40$ keV. Keep in mind that the pulsed beam current and energy increase for each duty cycle to maintain a fixed power setting according to Eqs. 8 and 9. In the following simulations, the spacecraft separation distance d is 12.5 m, center-to-center. The environment parameters used in the following discussion are listed in Table 1. These parameters correspond to $Kp = 6$ and $LT = 4$. This environment was chosen because previous research had shown that the ET performed better in an active environment (Hughes and Schaub, 2015b; Hughes and Schaub, 2017b).

Because the peak electrostatic force – not considering charging time – increases roughly linearly as the duty cycle decreases (per Eqs. 9 and 2), the average force over a pulsing period also increases as the duty cycle decreases. Charging, however, takes a certain amount of time. At some point, the duty cycle will become so short that the spacecraft will not have time to reach potentials greater than those resulting from the next largest duty cycle. Thus, the hypothesis is formed that there exists an optimal duty cycle such that the electrostatic force is maximized for a given space environment.

3.1. Determining an optimal duty cycle

Fig. 2 illustrates the charging response and the resulting force for duty cycles of ranging from 1 % to 10 % to try to numerically determine the duty cycle that minimizes the electrostatic force. Fig. 2 shows the simulation repeated for 5 linearly spaced duty cycles from 1 % to 10 %, with the exception of Fig. 2d, which has 50 duty cycle points. It is immediately evident in Fig. 2d that the hypothesis that there exists a duty cycle such that the electrostatic force is maximized is true; the force is maximized at a duty cycle of 4.489 %. Note that this value is approximate. The non-smooth behavior of the average force arises from averaging over the full duty cycle after solving for the spacecraft potentials with a stiff ODE solver. Because the solver adaptively adjusts its time steps to improve computational efficiency, it used more time steps in the pulsed portion of the cycle for some duty cycles than for others. As a result, the pulsed region was effectively weighted more heavily in the averaging process, leading to the observed non-smoothness.

The maximum average force (MAF) as seen in the figure is still on the order of mN, so how much of an effect does this optimization really have on the time to achieve ΔV? The ΔV required to successfully re-orbit the spacecraft

Table 1
Plasma parameters.

Particle	Parameter			
Type	T_1 (eV)	T_2 (eV)	n_1 (cm^{-3})	n_2 (cm^{-3})
Electron	1	2400	1	1.25
Ion	50	8100	0.01	0.95

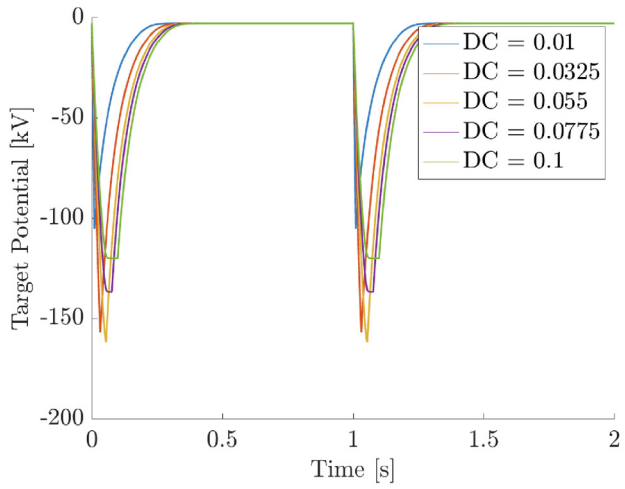

(a) Target potential over time

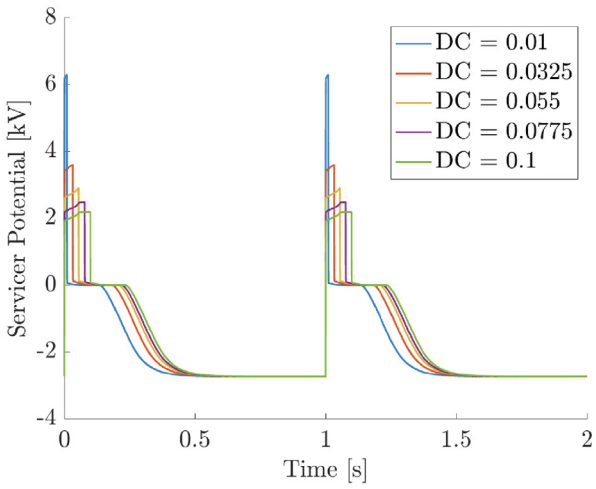

(b) Servicer potential over time

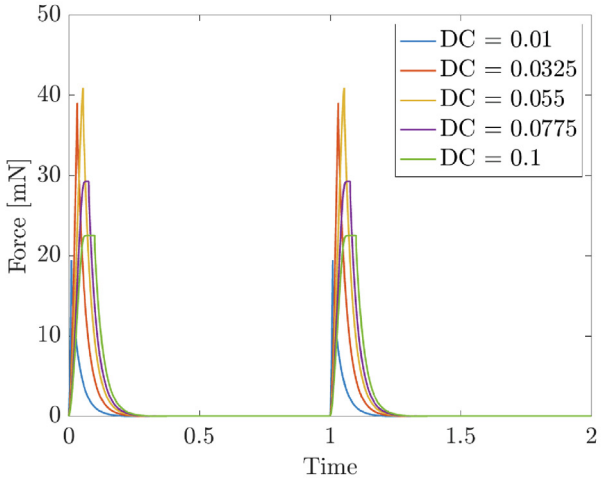

(c) Force over time

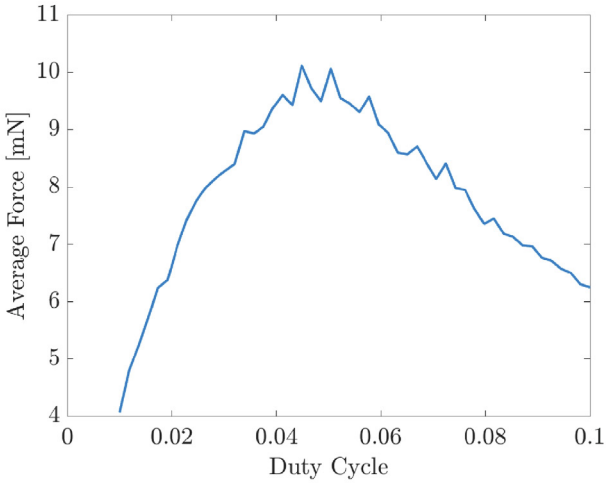

(d) Average force versus duty cycle

Fig. 2. Coupled effects of the electrostatic force for duty cycles ranging from 1 % to 10 %.

can be calculated assuming a Hohmann transfer (Vallado, 2001; Schaub and Junkins, 2018) from GEO to the graveyard orbit. GEO is located at approximately $r_1 = 42164.1$ km from the center of Earth and the graveyard orbit necessitated by laws in place by the Federal Communications Commission is $r_2 = r_1 + 300$ km (de Selding, 2004). Then, ΔV is found to be 10.88 m/s. This estimate agrees with other calculations for the ΔV to re-orbit GEO spacecraft, which use 11 m/s (Paganucci et al., 1997).

The resulting average electrostatic force at each duty cycle is substituted into Eq. (4) to obtain the required F_T to maintain a constant separation distance. Then, Eq. (5) is rearranged to find t_{burn}. The specific impulse I_{sp} of the propulsion system is 4190 s, which is the same I_{sp} as NASA's NEXT ion thruster (Glenn Research Center, YYYY). Results show that the specific impulse I_{sp} has a negligible effect on the burn time with such small forces. For a continuous beam, the average electrostatic force is 0.5271 mN, which results in a burn time of 93.39 days. Fig. 3 shows how the duty cycle affects the burn time to achieve ΔV for duty cycles ranging from 1 % to 10 %. The pulsed e-tractor maximum force achieved is an order of magnitude stronger than the electrostatic force for the continuous beam, at 10.12 mN. This results in a burn time of only 4.865 days, a twenty-fold reduction in reorbiting time compared to the continuous beam case with the same average power.

3.2. Hazard of field emission due to high potentials

When a conducting surface is charged to adequately high potentials such that its electric field is sufficiently enhanced, it may self-emit electrons in a phenomenon called field emission. Field emission does not stop electrostatic charging, but it becomes an additional current trying to reduce the target vehicle's negative potential that must be accounted for. Field emission is modeled using the Fowler–Nordheim (FN) equation (Fowler and Nordheim, 1928)

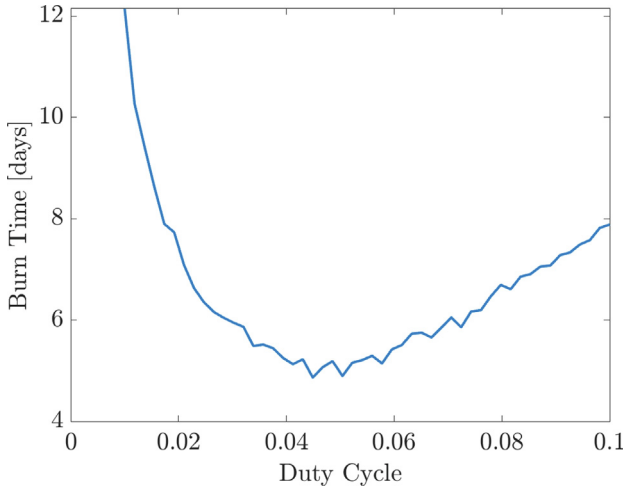

Fig. 3. Burn time versus duty cycle.

$$J(\varepsilon) = A\frac{\varepsilon^2}{\phi}\exp -\frac{B\phi^{3/2}}{\varepsilon} \tag{13}$$

where J is the emission current density, A and B are constants represented by $A = \frac{1.54\times10^{-6}}{\phi}, B = 6.83\times10^{9}, \phi$ is the work function for the material, and ε is the electric field at the surface. In this study, the material is assumed to be aluminum, which has a work function $\phi = 4.8$ eV (Michaelson, 1977). The electric field E can be related the electric potential of the surface V with a simple geometry using (Forbes, 2001)

$$\varepsilon = \frac{\beta V}{d} \tag{14}$$

where β is the field enhancement factor, which accounts for surface curvature or geometric effects that enhance the local electric field, and d is the separation in meters between the emitter and the counter-electrode. In this study, the spacecraft are assumed to be spherical, so β can be approximated as the ratio of d to the sphere's radius, R_T in this case. Substituting this into Eq. (14), we find that for the spherical target:

$$\varepsilon = \frac{V}{R_T}. \tag{15}$$

Then, substituting Eq. (15) into Eq. (13) leads to

$$J = A\frac{V^2}{R_T^2\phi}\exp -\frac{B\phi^{3/2}R_T}{V}. \tag{16}$$

For a highly charged spacecraft with surface imperfections, sharp corners, or pointed edges, field emission may interfere with its charging. In addition, the electric field of the servicer when in the proximity of these edges would enhance the total electric field, thus increasing the field emission from the target. The interaction of the electric fields can be roughly modeled by

$$\varepsilon = \varepsilon_T + \varepsilon_S = \frac{V_T}{R_{\text{tip}}} + \frac{V_S}{d - R_T} \tag{17}$$

where R_{tip} is the radius of the emitting tip.

When working with these high electrostatic potentials, a concern was that field emission could induce arcing between the spacecraft when the electric field at an asperity on the target became sufficiently high. This hypothesis is assessed in the same plasma parameters as before, $Kp = 6$ and $LT = 4$. The target and servicer have the same radii, but a very small sphere at the surface of target facing the servicer represents an emitting tip. The radius of this third sphere is simulated at $R_{\text{tip}} = 1$ μm, 5 μm, 10 μm, 30 μm, and 50 μm. It is assumed that because the servicer is charged positively, it will absorb all of the current that may be emitted from the target. Any secondary or backscattered electrons that may result from this field emission current on the servicer are not accounted for in this study. The electric field is calculated using Eq. (17). This result is used to compute the emitted current density using Eq. (13). Finally, the emitted current is calculated with $I_{\text{FE}} = J(4\pi R_{\text{tip}}^2)$.

Fig. 4 shows the results of the pulsed beam at 5 % duty cycle considering the field emission current. The varying R_{tip} are shown as colored solid lines and the case where field emission is not considered is shown as a black dashed line. It can be observed in Fig. 4a that field emission due to small asperities results in decreased charging. With the tip radius of 1 μm, the target charges to only −6.4 kV. On the other hand, the target charges to −165 kV when the tip radius is 50 μm, which is equivalent to the charging of the target without accounting for field emission. This corresponds to the magnitude of emitted current at each radius, shown in Fig. 4d. As the radius of the tip increases, the amount of emitted current decreases. At 50 μm, the emitted current is near zero. Likewise, the servicer charges negatively when impacted by the emitted current, as seen in Fig. 4b. For smaller radii, this effect is more profound since there is more current emitted from the tip.

Notably, these time-varying results show that arcing is not a concern. While field emission reaches relatively high currents for small tip radii, the current density remains low. The current density does not exceed 10^{-11} A/m^2. This maximum current density interestingly occurs for the 30 μm radius, but all of the radii reach similar maxima. Therefore, even though the target charges to extremely large potentials, the 50 μm radius tip does not pose a risk of arcing. Moreover, the 50 μm radius tip mitigates decreased charging related to field emission and prevents the servicer from reaching negative potentials. This indicates that field emission is only a concern for small enough geometrical features.

Fig. 5 compares the resulting forces from pulsed beam charging and continuous beam charging considering field emission. The forces for the pulsed beam, seen in Fig. 5a, reflect the decreased charging for small tip radii observed in Fig. 4. When $R_{\text{tip}} = 1$ μm, the MAF is only 0.05 mN, while at 50 μm the MAF is 10.5 mN (this value being greater than the previously noted peak force is the result

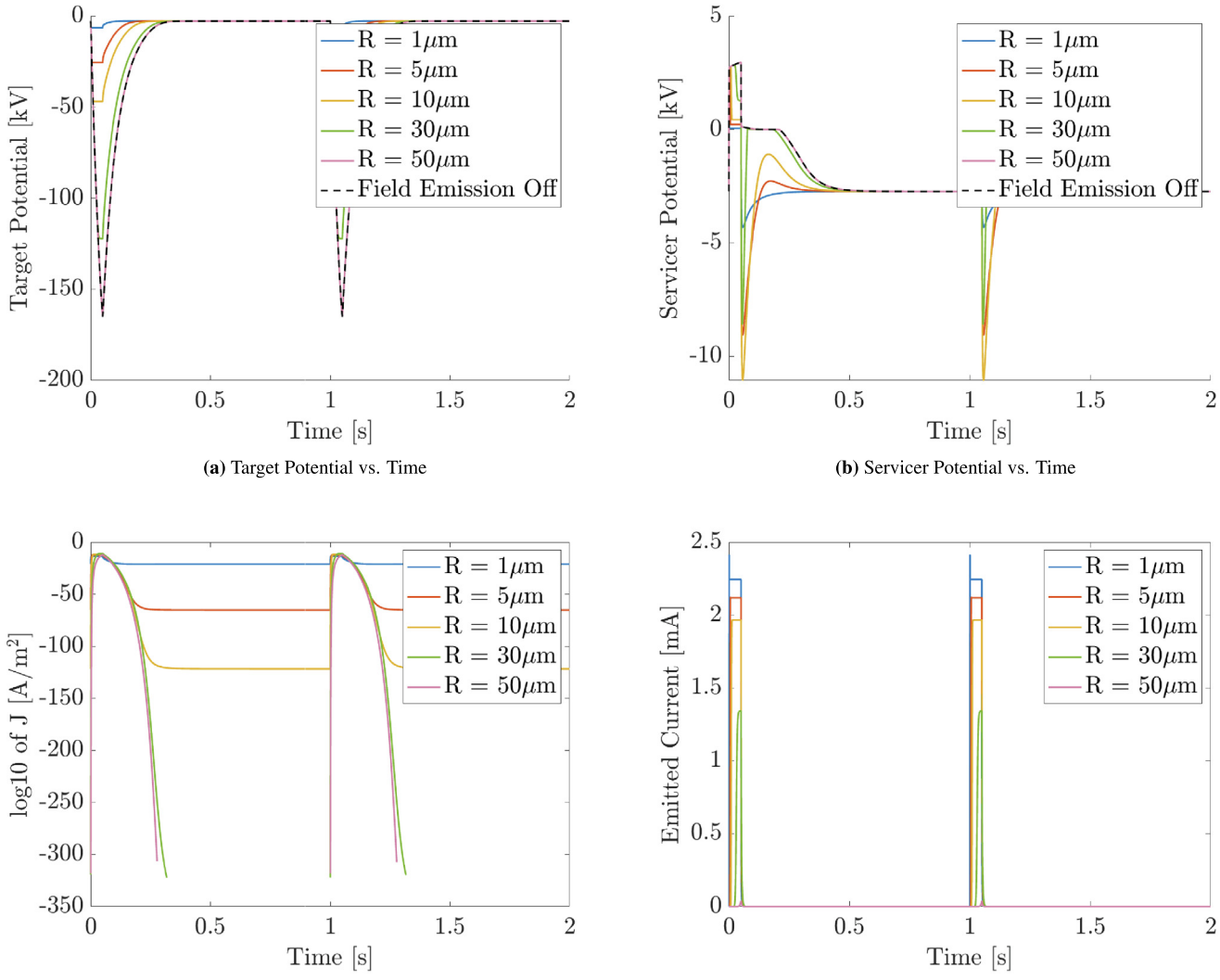

(a) Target Potential vs. Time

(b) Servicer Potential vs. Time

(c) log10 of Current Density vs Time

(d) Emitted Current vs Time

Fig. 4. Coupled charging results with field emission at duty cycle 5 %.

of errors inherent to the integrator, but the interpretation is the same). For the continuous beam, shown in Fig. 5b, field emission ceases to have an impact for larger tip radii, in this case greater than 10 μm. The average force levels out at around 0.52 mN, similarly to the previous result that did not account for field emission. Despite being severely depleted at smaller radii, the average force remains greater for the pulsed beam than that for the continuous beam. This is illustrated in Fig. 5c, where the average force for the pulsed beam for 100 linearly spaced radii from 1 to 10 μm is shown in blue and that for the continuous beam is colored red. At 1 μm the forces are comparable, though the pulsed beam is still slightly stronger. As the radius increases, the pulsed beam quickly becomes substantially more effective than the continous beam. Due to increased numerical precision used in Fig. 5c than in Fig. 5b, it can be seen that the increased tip size actually stops having an effect on the MAF for the continuous beam at around 8.5 μm rather than 10 μm.

However, recent experimental trials illustrate that increasing the e-beam current can offset the limiting effect of field emission (Walker and Schaub, 2024). This is because the e-beam current does not govern the maximum charging potential of the target, but instead allows the e-beam to dominate over other charging sources. Thus, the field emission current does not change because the potential of the target does not change, but the e-beam current is now more dominant. Thus, high kilo-volt potential levels are achievable even with field emission. A detailed study of this requires account for the spacecraft shape, surface materials, separation distance and relative orientation and is beyond the scope of this study.

For the remainder of this study, the pulsed beam is investigated without accounting for field emission.

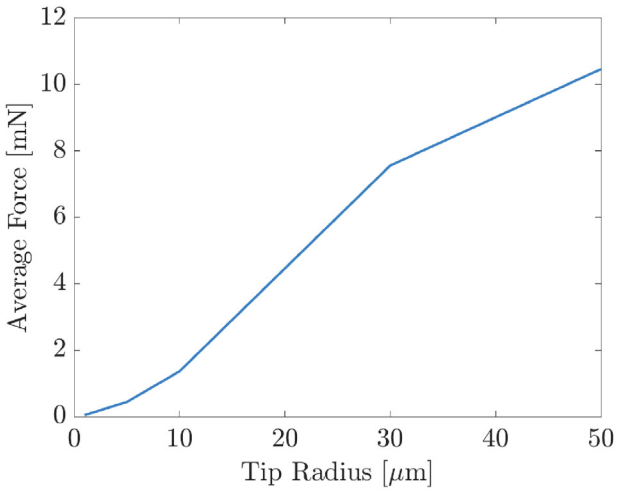

(a) Pulsed Beam

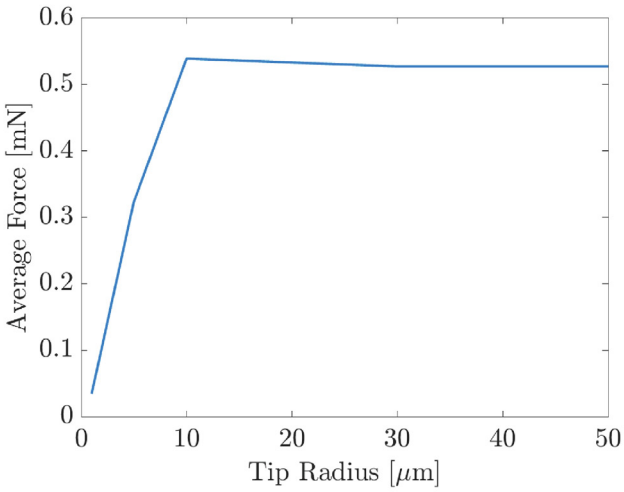

(b) Continuous Beam

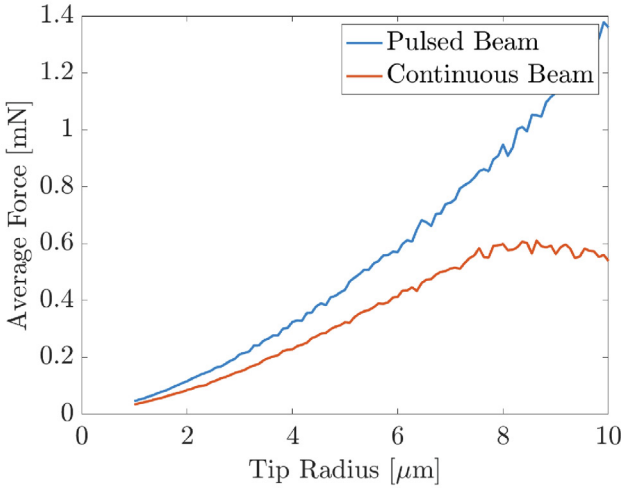

(c) Comparison at $R_{tip} = 1 - 10\mu$m

Fig. 5. Force vs. tip radius for the pulsed beam and continuous beam.

3.3. Effect of the photoelectron current

The photoelectron current is a positive current on a spacecraft that results from the photons from the sun exciting the electrons on the spacecraft surface. In the previous section, the target is assumed to be in eclipse, so this current was not taken into account. This was in order to provide an adequate picture of the optimal duty cycle. However, in the magnetosphere, the photoelectron current often dominates over the other ambient currents (protons, electrons, and resulting secondary and back-scattered currents) (Lai, 2012, Chapter 7). As a result, GEO spacecraft in sunlight are usually charged up to a few volts positive. GEO spacecraft are rarely in eclipse; the ATS-5 spacecraft, which was in an equatorial geosynchronous orbit, only entered eclipse for 30 min each night for a period of 3 to 4 weeks on either side of an equinox (DeForest, 1972). Thus, the photoelectron current is crucial to include when discussing GEO spacecraft.

Fig. 6 shows the MAF as a function of the percent of the target spacecraft's projected area surface that is exposed to sunlight. The MAF is found by iterating over the duty cycle to find the one that produces the minimum force in the same process that was used in the previous section. Fig. 6 illustrates how increasing the amount of surface exposed to the sun, and thus increasing the photoelectric current, reduces the magnitude of the MAF. The projected area of the servicer is assumed to remain fully exposed to sunlight, so it does not charge negatively due to the environment while the e-beam is powered off. Fig. 6 essentially simulates how the servicer's shadow on the target affects the electrostatic force between them. When the target's projected area is fully exposed to sunlight, the MAF is 2.900 mN, compared to 12.71 mN in eclipse. However,

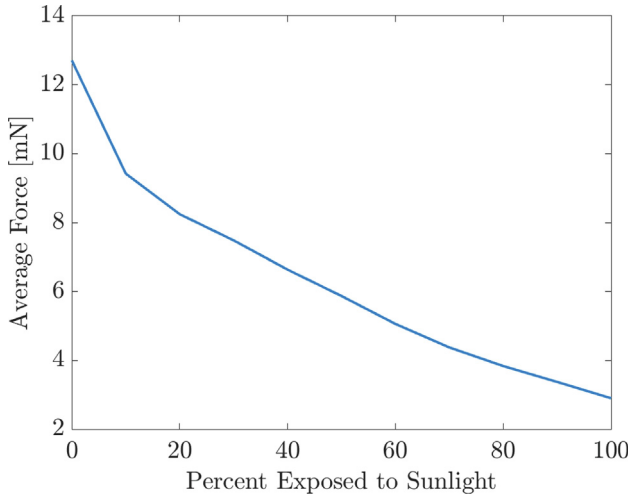

Fig. 6. Maximum average force versus percent sun exposure of the projected area.

the pulsed beam in full sun still performs significantly better than the continuous beam in eclipse (MAF = 0.5271 mN).

To further emphasize the effectiveness of the pulsed electron beam, Fig. 7 shows the charging and force responses for duty cycles of 10 %, 30 %, 50 %, 70 %, and 90 % in full sunlight. Fig. 7a shows that the target does not charge adequately negative for the duty cycles greater than 10 %. While there is an initial pulse for the 30 % duty cycle, this is because the e-beam current acts more quickly on the spacecraft than the environment. Thus, after the first pulse, the effect of the environment is in full effect. The lack of charging for higher duty cycles demonstrates the dominance of the photoelectric current compared to the other currents, including the e-beam current. As a result, the force is consistently near-zero for the higher duty cycles, as seen in Fig. 7c. Therefore, in order to even generate an electrostatic force with spacecraft of these sizes in this environment, the pulsed electron beam must be employed.

4. Effect of the nominal GEO environment on peak force

The plasma environment in GEO is constantly changing as a result of geomagnetic storms and substorms, which accelerate protons and electrons to high energies and inject them into synchronous altitudes. In the previous sections, the plasma parameters were those shown in Table 1, which correspond to $Kp = 6$ and $LT = 4$. As the plasma environment varies, it is of interest to investigate the impact the changing environment has on the electrostatic force enhancement obtained by pulsing the e-beam.

Fig. 8a shows the MAF as a function of the Kp index at $LT = 4$. The Kp index varies from $Kp = 0$ to $Kp = 6$. In reality, the Kp scale goes up to $Kp = 9$, but less than 5 % of days per 11-year solar cycle reach values greater than $Kp = 6$ (Noaa space weather scales, YYYY). In addition, we can recognize the pattern and make adequate predictions about the force enhancement during more severe solar storms. The key observation is that the MAF increases with K_p index. In other words, the pulsed electron beam performs better during active periods, which corroborates results from previous research (Hughes and Schaub, 2015b; Hughes and Schaub, 2017b). The data in Fig. 8a includes the photoelectron current at full sun exposure. At $K_p = 0$, the MAF is near zero, which is likely a result of the currents from the cold, dense plasma that is present dominating the electron beam current. The duty cycles used to find the MAF ranged from 1 % to 10 %. Some duty cycles smaller than 1 % were simulated, but due to the time required to charge up the spacecraft, the optimal duty cycle for these conditions falls in the 1 % to 10 % range. (see Fig. 9).

Fig. 8b, which shows the minimum average force as a function of LT at $Kp = 6$, follows the expected pattern based on the results of Fig. 8a. Around local midnight ($LT = 24$) the MAF decreases quickly, peaking during the early morning hours. Then, the plasmasphere particles move back into GEO and the cold, dense particles quickly dominate over the electron beam current. The near-zero forces seen in both Fig. 8b and 10b, which shows the same results but in eclipse, indicate that geomagnetic activity is essential for ET function at the current and voltage used here. However, stronger e-beams may provide the currents and energies necessary to function in even quiet environments.

5. Effect of electron beam power on peak force in quiet environments

To combat the cold plasmasphere particles that mitigate active charging during quiet periods in GEO, e-beams with greater fixed powers are explored. In the previous scenarios, the continuous beam parameters were fixed at $I = 520$ μA and $E = 40$ keV, which is equivalent to a beam power of $P = 20.8$ W. At this power setting, the electrostatic force was near-zero during quiet periods. The potential of the target spacecraft is limited by the pulsed energy of the e-beam. For example, at a duty cycle of 1 %, the pulsed energy of the e-beam is $40\ \text{keV}/\sqrt{0.01} = 400$ keV. Thus, the target could charge to a maximum of 400 V. However, for such small duty cycles, the time it takes for the spacecraft to charge prevents it from reaching its maximum potential in the period that the e-beam is turned on. The spacecraft can be charged more quickly by increasing the e-beam current.

Fig. 10 shows the effect of increasing the continuous beam current in the varying bi-Maxwellian environment for duty cycles ranging from 1 % to 10 % and a pulsing frequency of 1 Hz. In Fig. 10a, the local time is fixed at $LT = 4$, and in Fig. 10b, the Kp index is fixed at $Kp = 6$. The spacecraft are exposed to full sunlight. The results show how increasing the e-beam current allows the electrostatic force to grow as a result of the faster charging

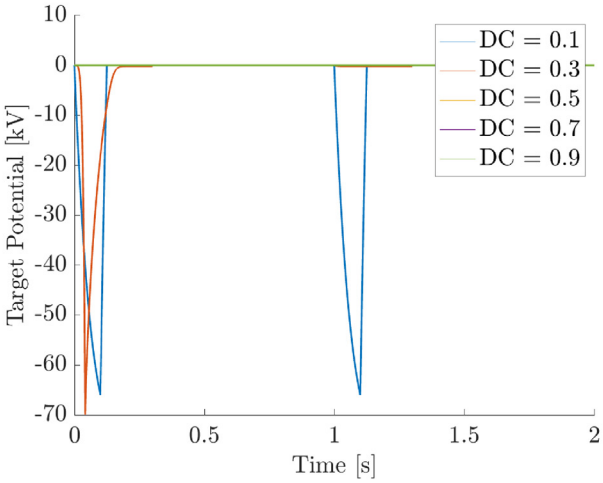

(a) Target potential over time

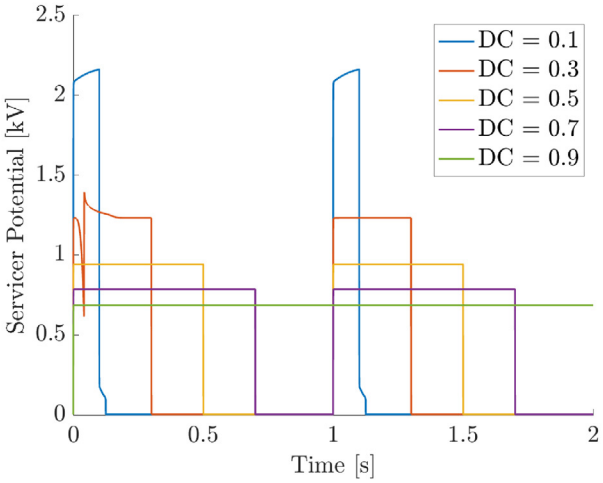

(b) Servicer potential over time

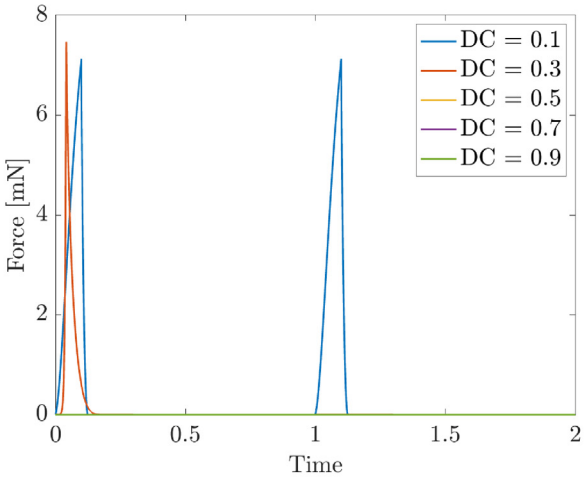

(c) Force over time

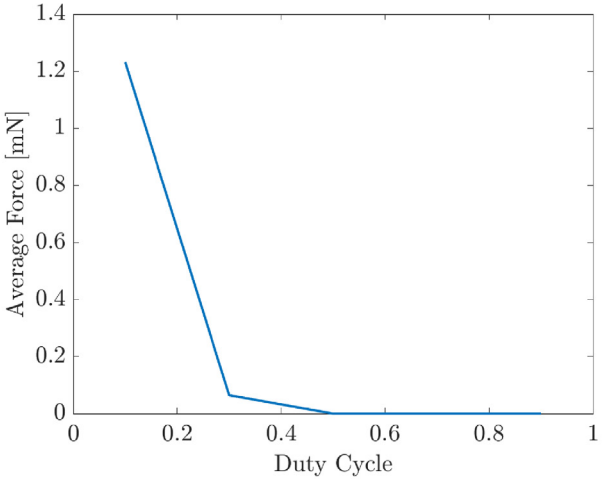

(d) Average force versus duty cycle

Fig. 7. Coupled effects of the electrostatic force for duty cycles ranging from 10 % to 90 % in full sunlight.

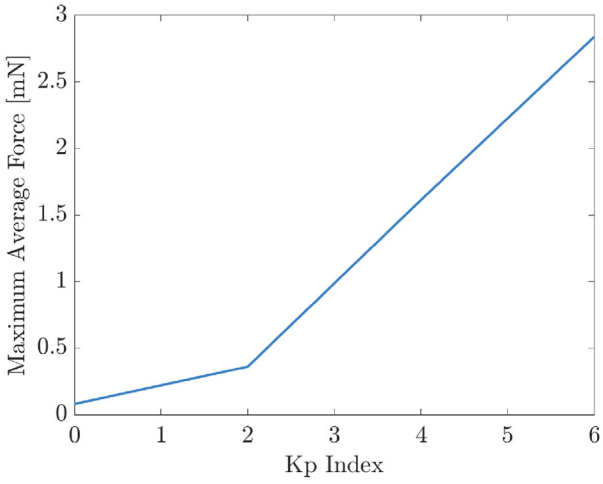

(a) Kp index versus minimum average force

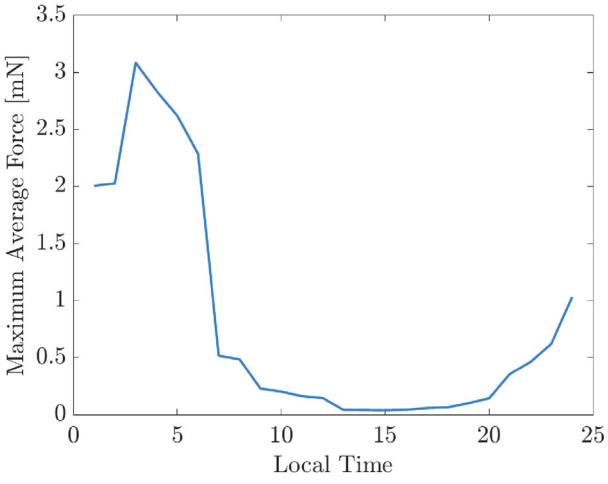

(b) Local time versus minimum average force

Fig. 8. Effect of a changing environment on minimum average force in sunlight.

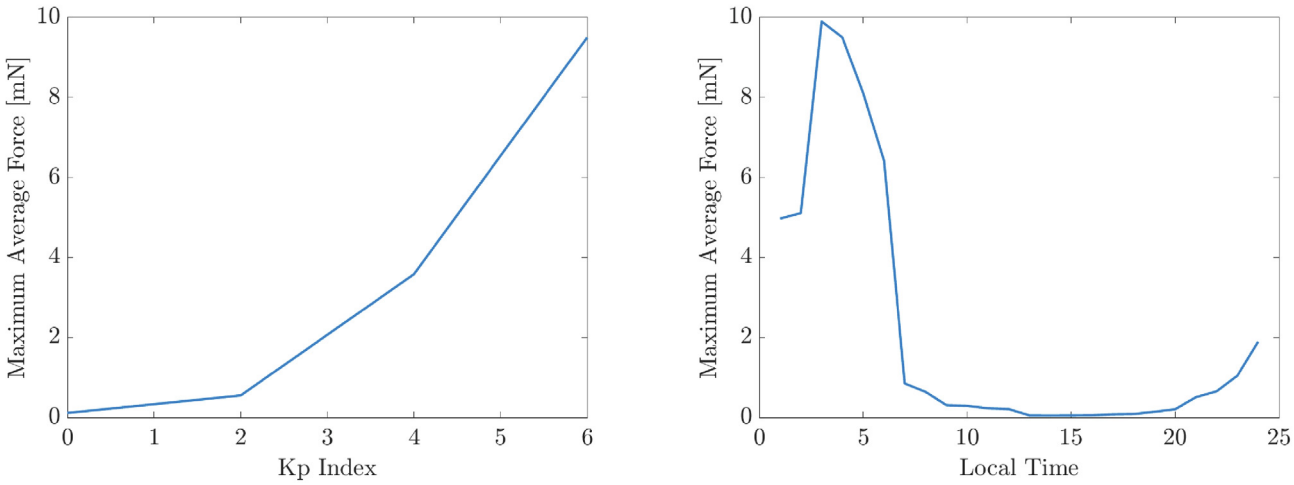

(a) Kp index versus minimum average force

(b) Local time versus minimum average force

Fig. 9. Effect of a changing environment on minimum average force in eclipse.

induced by higher currents. The maximum charging potential remains constant for each duty cycle, but the spacecraft is able to reach higher potentials in the period that the e-beam is turned on because it charges quicker. For example, in Fig. 10b, even at its minimum at $LT = 13$, the MAF for the 5 mA (continuous current value) e-beam is 2.591 mN. This value is nearly 5 times greater than the result for the continuous e-beam at 520 μA in optimal environmental conditions and in eclipse. In Fig. 10a, it is seen that at $Kp = 0$, charging is still difficult even with higher currents. However, the 5 mA e-beams still produces a MAF of 0.8261 mN, which is still greater than the optimal continuous case. At higher Kp indexes, each more powerful e-beam quickly overcomes the environment and performs better than the next highest power setting. Thus, using more powerful e-beams, specifically with greater current allowances, is a promising solution to overcoming environmental challenges.

Fig. 11 illustrates the charging and force responses of the spacecraft at duty cycles ranging from 1 % to 10 % at a pulsing frequency of 1 Hz for a continuous beam current of $I = 5$ mA in sunlight. It is immediately evident from Fig. 11d that the result is not optimized. At a the duty cycle of 1 %, the beam energy is 40 keV/$\sqrt{0.01}$ = 400 keV. Thus, it is also evident that the spacecraft does not have time to charge to its maximum potential (400 kV) in the time that the e-beam is powered on. This means that for smaller duty cycles, the spacecraft will also not charge to its maximum possible potential. It was previously concluded that an optimal duty cycle will exist such that the force is maximized. However, to decrease the duty cycle would continue to increase the e-beam power required. Commercially

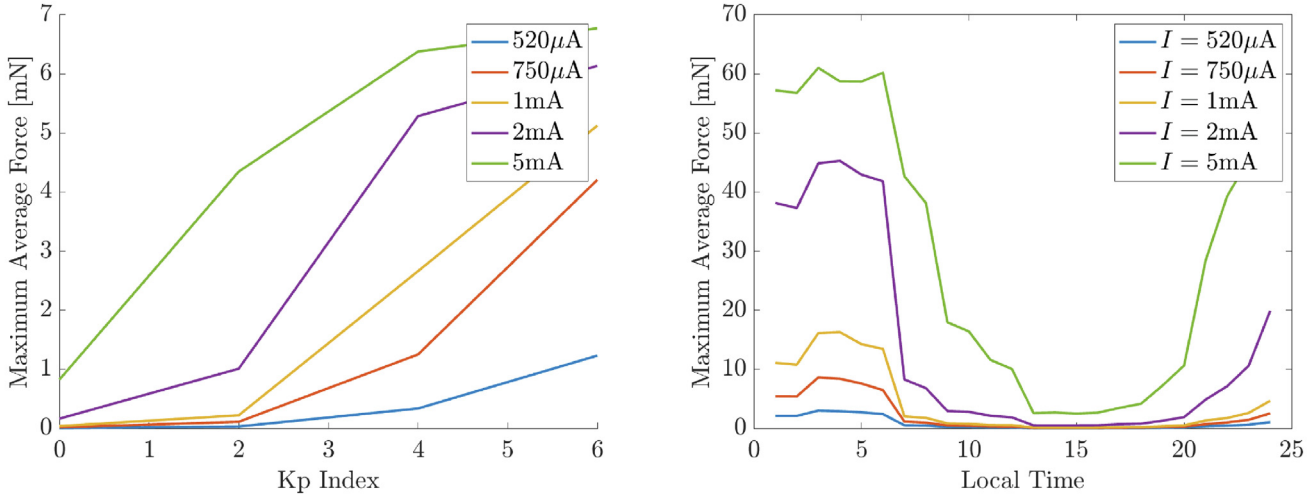

(a) Maximum average force as a function of Kp

(b) Maximum average force as a function of LT

Fig. 10. Effect of changing e-beam current for duty cycles from 1 % to 10 %.

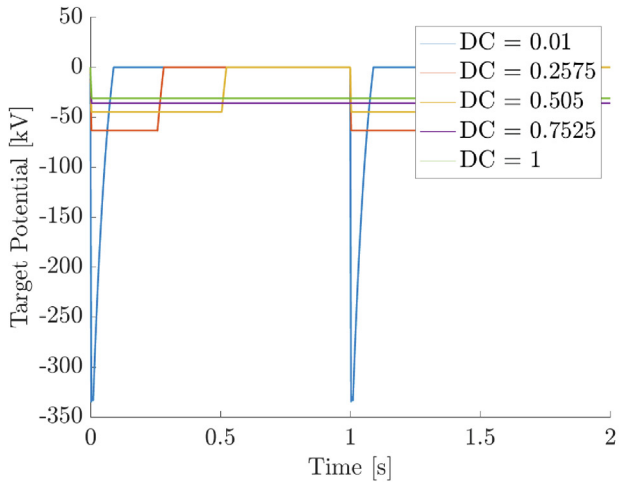

(a) Target potential over time

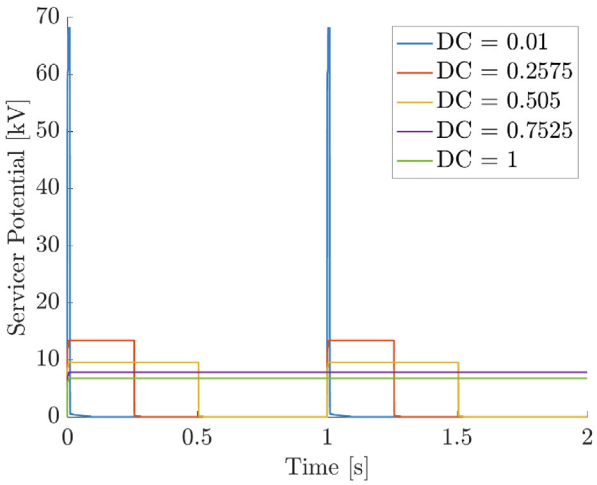

(b) Servicer potential over time

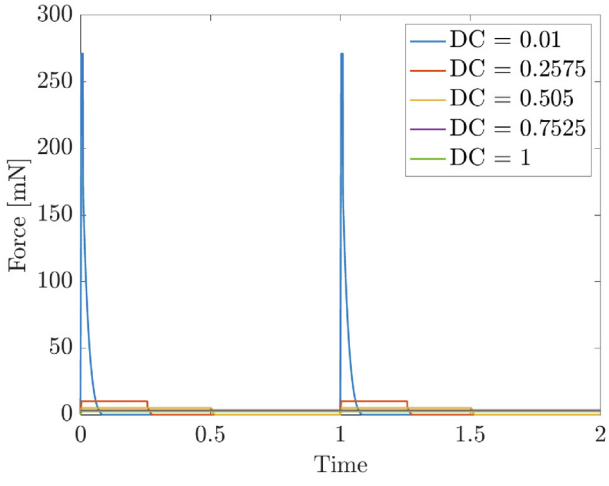

(c) Force over time

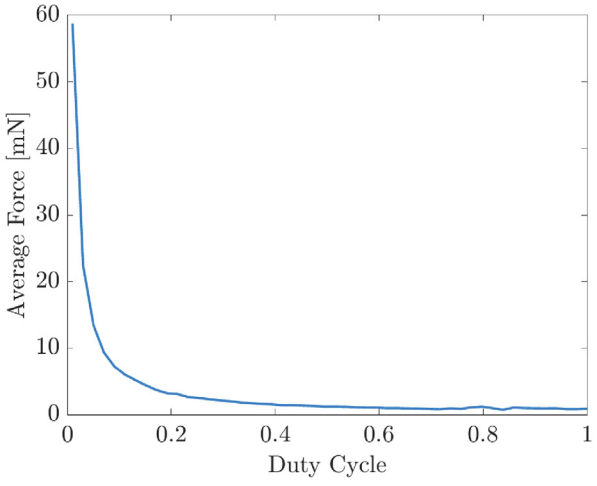

(d) Average force versus duty cycle

Fig. 11. Coupled effects of the electrostatic force for duty cycles ranging from 1 % to 10 % at $I = 5$ mA.

available e-beams have powers of up to only 100 keV,[3] with those used in space applications at only 20 keV. Thus, it is not practical to explore duty cycles that would require these exceedingly high energy levels. Likewise, this configuration requires a pulsed e-beam current of 5 $\text{mA}/\sqrt{0.01} = 50$ mA, where commercial e-beams allow currents up to 20 mA and ones currently in development allow currents up tot 30 mA. The e-beam limitations will be a challenge for overcoming environmental charging obstacles in application.

6. Conclusion

The effects of pulsing an electron beam (e-beam) are analyzed in the context of the electrostatic tractor concept for GEO space weather environments. The goal of the study is to maximize the electrostatic force magnitude to generate to the greatest attractive force between the servicer and target spacecraft. Decreasing the duty cycle decreases the average electrostatic force until the duty cycle becomes small enough such that the target cannot fully charge in the time that the e-beam is turned on. As a result, the electrostatic force decreases when the duty cycle decreases beyond an optimal value. The optimal duty cycle results in a force that can be orders of magnitude greater than that of a continuous beam for the same mean e-beam power consumption. The burn time to achieve the ΔV required to transfer to a graveyard orbit is then also orders of magnitude less than that using a continuous beam. The optimal duty cycle is dependent on the e-beam parameters and external factors such as plasma environment and exposure to sunlight and would need to be determined on a case-to-case basis.

Overall, the pulsed electron beam presents a promising solution to optimizing debris removal in GEO. However, some limitations still exist. While in an eclipse, the target

[3] https://www.kimballphysics.com/product/egh-8201-egps-8201/.

spacecraft may charge to over −100 kV, which could lead to field emission that must be compensated for. During quiet periods in GEO, the spacecraft are limited in their charging by the very cold and more dense plasmasphere particles that may extend into the GEO regime. To over come this obstacle, more powerful electron beams are explored. However, commercially available electron beams that currently exist have maximum beam energies and currents that may prevent charging to the necessary potentials to overcome the changing environment.

Declaration of competing interest

The authors declare the following financial interests/personal relationships which may be considered as potential competing interests: Amy Haft reports financial support was provided by Air Force Office of Scientific Research. If there are other authors, they declare that they have no known competing financial interests or personal relationships that could have appeared to influence the work reported in this paper.

Acknowledgment

The authors would like to thank Julian Hammerl for his spacecraft charging model and his guidance using the pulsed beam simulation. The authors would also like to thank Ethan Weber for his contributions to studying field emissions. This work was supported by the U.S. Air Force Office of Scientific Research under grant FA9550-23-S-0570.

References

Noaa space weather scales ( ).https://www.swpc.noaa.gov/noaa-scales-explanation.

Anderson, P.C., 2012. Characteristics of spacecraft charging in low earth orbit. J. Geophys. Res.: Space Phys., 117(A7).https://agupubs.onlinelibrary.wiley.com/doi/abs/10.1029/2011JA016875. doi: 10.1029/2011JA016875. arXiv:https://agupubs.onlinelibrary.wiley.com/doi/pdf/10.1029/2011JA016875.

Aslanov, V., 2019. Detumbling attitude control analysis considering an electrostatic pusher configuration. J. Guid., Control, Dynam. 2, 900–909.

Aslanov, V., 2020. Dynamics and control of a two-spacecraft coulomb formation: challenges and prospects. J. Phys.: Conf. Ser.

Aslanov, V., Schaub, H., 2018. Prospects of touchless space debris detumbling using an electrostatic pusher configuration. In: 69th International Astronautical Congress (IAC).

Aslanov, V., Yudintsev, V., 2018. Motion control of space tug during debris removal by a coulomb force. J. Guid., Control, Dynam. 41 (7).

Bennett, T., Schaub, H., 2015. Touchless electrostatic three-dimensional detumbling of large axi-symmetric debris. J. Astronaut. Sci. 62, 233–253.

Bennett, T., Schaub, H., 2018. Contactless electrostatic detumbling of axi-symmetric geo objects with nominal pushing or pulling. Adv. Space Res. 62, 2977–2987.

Champion, K., Schaub, H., 2023. Electrostatic potential shielding in representative cislunar regions. IEEE Trans. Plasma Sci. 51, 2482–2500.

Davis, V., Gardner, B., Mandell, M., 2016. Nascap-2k version 4.3 users manual. Leidos Holdings San Diego, CA, USA, Tech. Rep. AFRL-RVPS-TR-2017-0002.

de Selding, P., 2004. Fcc enters orbital debris debate. Space News Business Report.

DeForest, S.E., 1972. Spacecraft charging at synchronous orbit. J. Geophys. Res. 77.

Denton, M.H., Thomsen, M.F., Korth, H., et al., 2005. Bulk plasma properties at geosynchronous orbit. J. Geophys. Res.: Space Phys.

Forbes, R.G., 2001. Field emission: New theory for the derivation of emission area from a fowler-nordheim plot. J. Vacuum Sci. Technol. B: Microelectron. Nanometer Struct. Process., Measur., Phenom. 19, 1280–1286.

Fowler, R. H., Nordheim, L., 1928. Electron emission in intense electric fields. Proc. Roy. Soc. A: Math., Phys. Eng. Sci., 119, 173–181.

Glenn Research Center ( ). Gridded ion thrusters (next-c): Next ion engine test firing. Https://www1.grc.nasa.gov/space/sep/gridded-ion-thrusters-next-c/.

Guillemant, S., Génot, V., Matéo-Vélez, J.-C., et al., 2012. Solar wind plasma interaction with solar probe plus spacecraft. Ann. Geophys. 30 (7), 1075–1092. https://doi.org/10.5194/angeo-30-1075-2012, URL: https://angeo.copernicus.org/articles/30/1075/2012/.

Haft, A., Schaub, H., 2024. Electrostatic tractor effectiveness in a non-maxwellian geo plasma environment. In: In AAS Astrodynamics Specialist Conference.

Hammerl, J., Schaub, H., 2024a. Coupled spacecraft charging due to continuous electron beam emission and impact. J. Spacecr. Rock.

Hammerl, J., Schaub, H., 2024b. Reduced order spacecraft charging models for electrostatic proximity operations. IEEE Trans. Plasma Sci. 52 (11), 5402–5413.

Hogan, E., Schaub, H., 2013. Relative motion control for two-spacecraft electrostatic relative motion control for two-spacecraft electrostatic orbit corrections. J. Guid., Control, Dynam. 36 (1).

Hogan, E., Schaub, H., 2015a. Impacts of tug and debris sizes on electrostatic tractor charging performance. Adv. Space Res. 55, 630–638.

Hogan, E.A., Schaub, H., 2015b. Impacts of hot space plasma and ion beam emission on electrostatic tractor performance. IEEE Trans. Plasma Sci. 43.

Hughes, J., Schaub, H., 2017a. Orbital and storm time analysis of the pulsed electrostatic tractor. In: European Conference on Space Debris.

Hughes, J., Schaub, H., 2017b. Prospects of using a pulsed electrostatic tractor with nominal geosynchronous conditions. IEEE Trans. Plasma Sci. 45 (8).

Laakso, H., Opgenoorth, O., Wygant, J., et al., 1997. Electron density distribution in the magnetosphere. In: Correlated Phenomena at the Sun, in the Heliosphere and in Geospace. 31st ESLAB Symposium.

Lai, S.T., 2011. Fundamentals of Spacecraft Charging. Princeton University Press. https://doi.org/10.2307/j.ctvcm4j2n.

Lai, S.T., 2012. Fundamentals of Spacecraft Charging. Princeton University Press.

Leahy, F., 2021. Sls-spec-159, cross-program design specification for natural environments (dsne).

Michaelson, H.B., 1977. The work function of the elements and its periodicity. J. Appl. Phys. 48.

Olsen, R.C., 1987. Record charging events from Applied Technology Satellite 6. J. Spacecr. Rock. 24 (4), 362–366. https://doi.org/10.2514/3.25925.

Ostrove, B., 2015. Average commercial communications satellite launch mass declines, again. Defense and Security Monitor.

Paganucci, F., Saccoccia, G., Scortecci, F., 1997. Method for re-orbiting a dual-mode propulsion geostationary spacecraft. URL: https://web.archive.org/web/20131110184645/http://www.patentgenius.-com/patent/5651515.html uS Patent 5651515A.

Pierrard, V., Botek, E., Ripoll, J.-F., et al., 2021. Links of the plasmapause with other boundary layers of the magnetosphere: Ionospheric convection, radiation belt boundaries, auroral oval. In: Front. Astron. Space Sci., p. 8.

Schaub, H., D. F. Moorer, J., 2012. Geosynchronous large debris reorbiter: Challenges and prospects. J. Astronaut. Sci., 59, 161–176.

Schaub, H., Jasper, L.E.Z., 2013. Orbit boosting maneuvers for two-craft coulomb formations. J. Guid., Control, Dynam.
Schaub, H., Junkins, J.L., 2018. Analytical Mechanics of Space Systems, 4th Edition. AIAA Education Series, Reston, VA.
Schaub, H., Sternovsky, Z., 2014. Active space debris charging for contactless electrostatic disposal maneuvers. Adv. Space Res. 53, 110–118.
Smythe, W.R., 1968. Static & Dynamic Electricity, 3rd Edition. McGraw Hill.
Stevenson, D., 2016. Electrostatic spacecraft rate and attitude control—experimental results and performance considerations. Acta Astranautica 119, 22–33.
Stevenson, D., Schaub, H., 2013. Multi-sphere method for modeling spacecraft electrostatic forces and torques. Adv. Space Res.
Tahir, A.M., Narang-Siddarth, A., 2018. Constructive nonlinear approach to coulomb formation control. In: AIAA Guidance Navigation and Control Conference.
Ting, W., Guangqing, X., Nan, Z., 2016. Reconfiguration and control of non-equal mass three-craft coulomb formation. J. Astronaut. Sci.
Trevor Bennett, E.H., Stevenson, Daan, Schaub, H., 2015. Prospects and challenges of touchless electrostatic detumbling of small bodies. Adv. Space Res. 56, 557–568.
Vallado, D.A., 2001. Fundamentals of Astrodynamics and Applications. Microcosm Press and Kluwer Academic Publishers.
Walker, J., Schaub, H., 2024. Development of experimental methods for active charge control using remote sensing methods. In: The 17th Spacecraft Charging and Technology Conference. Palais des Papes, Avignon, France.
Williams, D.J., 1985. Dynamics of the earth's ring current: theory and observation. Space Sci. Rev. 42, 375–396.
Yamamoto, U., Yamakawa, H., 2008. Two-craft coulomb-force formation dynamics and stability analysis with debye length characteristics. In: AIAA/AAS Astrodynamics Specialist Conference and Exhibit.